Special Issue

Ge–Fe Carbonyl Cluster Compounds: Ionic Liquids-Based Synthesis, Structures, and Properties

Silke Wolf,* Alexander Egeberg, Jens Treptow, and Claus Feldmann*[a]

Dedicated to Professor Bernd Harbrecht on the occasion of his 70th birthday.

Nine Ge–Fe carbonyl cluster compounds are prepared via ionic liquids-based synthesis. This includes the novel compounds [EMIm][Fe(CO)$_3$I(GeI$_3$)], [EHIm][Fe(CO)$_3$I(GeI$_3$)], [BMIm][GeI$_2${Fe(CO)$_4$}$_2$(μ-I)][AlCl$_4$]$_2$, [GeI$_2${Fe(CO)$_4$}$_2$(μ-I)][Fe(AlBr$_4$)$_3$], [BMIm]$_2$[(FeI$_2$)$_{0.75}${Fe(CO)$_2$I(GeI$_3$)$_2$}$_2$], and [EHIm][Fe(CO)$_4$(GeI$_2$)$_2$Fe(CO)$_3$GeI$_3$] as well as the previously reported compounds (Fe(CO)$_4$(GeI$_3$)$_2$, FeI$_4${GeI$_3$Fe(CO)$_3$}$_2$, and Ge$_{12}${Fe(CO)$_3$}$_8$(μ-I)$_4$ (EMIm: 1-ethyl-3-methylimidazolium, EHIm: 1-ethylimidazolium, BMIm: 1-butyl-3-methylimidazolium). With this series of compounds, a comparison of synthesis conditions and structural features is possible and, for instance, allows correlating the composition and structure of the respective Ge–Fe carbonyl cluster compounds with the type and acidity of the ionic liquid. With [EMIm][{GeI$_3$}$_2$Fe(CO)$_3$I], moreover, we can exemplarily show the thermal decomposition as a single-source precursor in the ionic liquid, resulting in bimetallic Ge–Fe nanoparticles with small size and narrow size distribution (7.0 ± 1.4 nm).

1. Introduction

Ionic liquids (ILs) have turned out to be suitable reaction media for the synthesis and crystallization of reactive carbonyl and cluster compounds.[1–3] Most relevant features of ILs are the high redox stability and the weakly-coordinating properties. Prominent examples include, for instance, □$_{24}$Ge$_{136}$ as a new modification of germanium (□ indicates non-occupied regular lattice sites),[4] [Hg$_4$Te$_8$(Te$_2$)$_4$]$^{8-}$ with a porphyrin-analogous structure,[5] or the Zintl-like cation [CuBi$_8$]$^{3+}$.[6] In addition to the redox stability and the weakly-coordinating properties, the inherent stabilization of compounds via cation-anion interactions as well as the presence of voluminous and inert cations/anions are further merits of ILs.[7] Aiming at carbonyl cluster compounds, even halide-coordinated species can be obtained, which were often denoted as highly labile due to the missing electronic and steric stabilization of alkyl or aryl ligands.[1–6]

Our studies on the reactivity and reactions of metal carbonyls have already demonstrated ILs to be powerful reaction media and resulted in various new carbonyl cluster compounds. Selected examples comprise the adamantane-type Fe$_4$Sn$_6$ cluster core in [{Fe(CO)$_3$}$_4${SnI}$_6$I$_4$]$^{2-}$,[8] the Ge$_{12}$Fe$_8$ germanium-iron cluster core in Ge$_{12}${Fe(CO)$_3$}$_8$(μ-I)$_4$,[9] [SnI$_8${Fe(CO)$_4$}$_4$]$^{2+}$ containing a highly coordinated Sn^{+II}I$_8$ subunit,[10] or an anti-(WCl$_2$)$_6$-like [(Pb$_6$I$_8$){Mn(CO)$_5$}$_6$]$^{2-}$ cluster.[11] Especially, reactions of Fe(CO)$_5$ or Fe$_2$(CO)$_9$ with Lewis-acidic metal iodides (e.g., SnI$_4$, GeI$_4$) resulted in a series of novel carbonyl cluster compounds that are specifically designated by the absence of alkyl and aryl ligands.[8–12] Thus, a synthesis of such highly labile compounds is possible although the electronic and/or sterical stabilization of alkyl/aryl ligands is missing.[13]

Aiming at carbonyl compounds, generally only few compounds were reported for a specific system and/or prepared via comparable experimental conditions. This situation can be ascribed to high chemical and thermal reactivity of carbonyl compounds. Hence, an examination of the relevant parameters to obtain the one or other composition and structure as well as a development of rational synthesis routes with controlled formation of specific compounds are difficult. For the system Ge–Fe, we could already realize three different carbonyl cluster compounds with Ge–Fe bonds. These are (Fe(CO)$_4$(GeI$_3$)$_2$, FeI$_4${GeI$_3$Fe(CO)$_3$}$_2$, and Ge$_{12}${Fe(CO)$_3$}$_8$(μ-I)$_4$,[9,12] which were all prepared by ionic-liquid-based synthesis. Based on the success of this synthesis route, we have examined the Ge–Fe system in more detail, resulting in six additional compounds: [EMIm][Fe(CO)$_3$I(GeI$_3$)], [EHIm][Fe(CO)$_3$I(GeI$_3$)], [BMIm][GeI$_2${Fe(CO)$_4$}$_2$(μ-I)][AlCl$_4$]$_2$, [GeI$_2${Fe(CO)$_4$}$_2$(μ-I)][Fe(AlBr$_4$)$_3$], [BMIm]$_2$[(FeI$_2$)$_{0.75}${Fe(CO)$_2$I(GeI$_3$)$_2$}$_2$], and [EHIm][Fe(CO)$_4$(GeI$_2$)$_2$Fe(CO)$_3$GeI$_3$] (EMIm: 1-ethyl-3-methylimidazolium, EHIm: 1-ethylimidazolium, BMIm: 1-butyl-3-methylimidazolium). The chemical synthesis and the structural characterization of in total nine Ge–Fe carbonyl cluster compounds now allows a comparison of the experimental conditions, structural features, and properties.

[a] Dr. S. Wolf, Dr. A. Egeberg, J. Treptow, Prof. Dr. C. Feldmann
Institut für Anorganische Chemie
Karlsruhe Institute of Technology (KIT)
Engesserstraße 15
76131 Karlsruhe (Germany)
E-mail: silke.wolf@kit.edu
claus.feldmann@kit.edu

Supporting information for this article is available on the WWW under https://doi.org/10.1002/open.202000254

Special Issue *An invited contribution to a Special Issue dedicated to Material Synthesis in Ionic Liquids.*

2. Results and Discussion

2.1. State-of-the-Art of Ge–Fe Carbonyl Compounds

According to the literature, carbonyls in the system Ge–Fe–*X* (*X*: Cl, Br, I) are generally rare and most often contain isolated Ge–Fe or Ge–Fe–Ge strings.[12,14–15] Such compounds were first presented by *Kummerer* and *Graham* and prepared by reaction of $Fe(CO)_5$ with GeX_4 in benzene.[14a] Few examples relate to larger Ge–Fe clusters with 5–8 metal atoms. This includes $[\mu^4$-$(^tBu_2MeSi)_4Ge_4\}]Fe(CO)_3$,[16] $Fe_3\{\mu^3$-$GeCo(CO)_4\}_2(CO)_9$,[17] or the cluster compounds $[Ge_{10}\{Fe(CO)_4\}_8]^{6-}$ and $Ge_{12}\{FeCp$-$(CO)_2\}_8\{FeCp(CO)_2\}$.[18] The latter contain Ge_{10} and Ge_{12} cluster cores that are stabilized by iron carbonyl and cyclopentadienyl (Cp) ligands.[18] These compounds were prepared by reaction of a very labile Ge(I)Br intermediate via co-condensation methods. So far, ILs were not used to prepare carbonyl cluster compounds in the Ge–Fe system.

As part of our previous work on the IL-based synthesis of carbonyl and/or cluster compounds, we have already realized $(Fe(CO)_4(GeI_3)_2$ (**I**), $FeI_4\{GeI_3Fe(CO)_3\}_2$ (**II**), and $Ge_{12}\{Fe(CO)_3\}_8(\mu$-$I)_4$ (**III**) in the Ge–Fe system (Figure 1).[9,12] These compounds were all obtained by reacting GeI_4 and $Fe_2(CO)_9$ in a mixture of [BMIm]Cl and $AlCl_3$ as IL ([BMIm: 1-butyl-3-methylimidazolium). In regard of the structural features, $(GeI_3)_2Fe(CO)_4$ (**I**) consists of two GeI_3 units that are connected by a square planar $Fe(CO)_4$ group with a linear Ge–Fe–Ge arrangement.[12] $FeI_4\{GeI_3Fe$-$(CO)_3\}_2$ (**II**) consists of two $GeI_2I_{1/2}$–$Fe(CO)_3I_{2/2}$ units that are interlinked via a distorted octahedral $FeI_{6/2}$ group.[12] After synthesis, $FeI_4\{GeI_3Fe(CO)_3\}_2$ decomposes on a timescale of several days in the mother lye to $(GeI_3)_2Fe(CO)_4$.[12] Finally, the germanium-iron cluster $Ge_{12}\{Fe(CO)_3\}_8(\mu$-$I)_4$ (**III**) contains a $Ge_{12}Fe_8$ cluster core, which consists of a central Ge_4 rectangle, two Ge_2 pairs, and four single Ge atoms (Figure 1). These different Ge species are interconnected by Fe atoms to the $Ge_{12}Fe_8$ cluster core, which also represents the one of the largest cluster cores in the Ge–Fe system known so far.[9]

2.2. New Ge–Fe Carbonyl Compounds

The novel Ge–Fe cluster compounds $[EMIm][Fe(CO)_3I(GeI_3)]$, $[EHIm][Fe(CO)_3I(GeI_3)]$, $[BMIm][GeI_2\{Fe(CO)_4\}_2(\mu$-$I)][AlCl_4]_2$, $[GeI_2\{Fe(CO)_4\}_2(\mu$-$I)][Fe(AlBr_4)_3]$, $[BMIm]_2[(FeI_2)_{0.75}\{Fe(CO)_2I(GeI_3)_2\}_2]$, and $[EHIm][Fe(CO)_4(GeI_2)_2Fe(CO)_3GeI_3]$ were as well obtained via IL-based synthesis. The experimental conditions and the structural features are discussed in the following.

$[BMIm]_2[(FeI_2)_{0.75}\{Fe(CO)_2I(GeI_3)_2\}_2]$ (**1**) was prepared by reacting GeI_4 and $Fe_2(CO)_9$ with Ph_3GeCl in a 1:1 mixture of [BMIm]Cl and $AlCl_3$. Moreover, Ph_3GeCl was added to influence the Ge:I ratio. After dissolution as Ph_3Ge^+ and Cl^-, the Ph_3Ge^+ cation preferentially binds iodine and was frequently obtained as insoluble Ph_3GeI subsequent to the reaction. The reduced amount of available iodine promotes the formation of Ge–Fe bonds. Thus, the synthesis results in red crystals of **1** (SI: Figure S1) together with bright red crystals of Ph_3GeI. After several days, the title compound starts to decompose even in the mother lye. After approximately two weeks, bright-red needles of the already known compound $Fe(CO)_4\{GeI_3\}_2$ (**I**) were formed. This finding is not surprising since $Fe(CO)_4\{GeI_3\}_2$ was also directly formed in absence of Ph_3GeCl.[12] **1** crystallizes in the monoclinic space group $P2_1/c$ and contains $[BMIm]^+$ cations and $[(FeI_2)_{0.75}\{Fe(CO)_2I(GeI_3)_2\}_2]^{2-}$ anions (Table 1, Figure 2). The synthesis of **1** can be rationalized by the following equation:

$$2\ Fe_2(CO)_9 + 4\ GeI_4 + Ph_3GeCl + 2\ [BMIm]^+ \rightarrow$$
$$[BMIm]_2[(FeI_2)_{0.75}\{Fe(CO)_2I(GeI_3)_2\}_2] +$$
$$14\ CO + 1.25\ Fe^{2+} + Cl^- + 0.5\ Ph_3GeI + 0.5\ Ph_3Ge^+$$

The 1:1 ratio of [BMIm]Cl and $AlCl_3$ as well as the presence of Ph_3GeCl turned out to be crucial. By increasing the [BMIm]-Cl:$AlCl_3$ ratio, **2** is formed, whereas – as discussed above – $Fe(CO)_4\{GeI_3\}_2$ (**I**) is formed in absence of Ph_3GeCl.[12] In addition to single crystal structure analysis, the composition of **1** was verified by energy-dispersive X-ray spectroscopy (EDXS). The observed Fe:Ge:I ratio of 4:2.5:15.1 (scaled on Ge) is well in

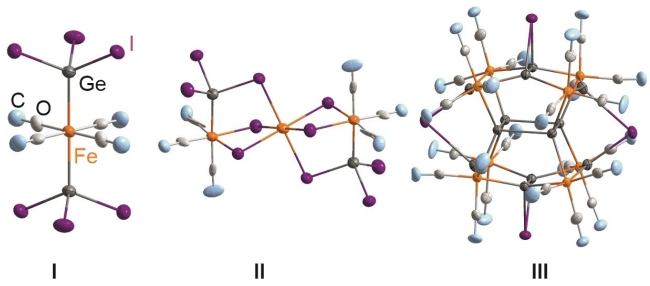

Figure 1. Ge–Fe building units in the previously reported carbonyl cluster compounds $(GeI_3)_2Fe(CO)_4$ (**I**), $FeI_4\{GeI_3Fe(CO)_3\}_2$ (**II**), and $Ge_{12}\{Fe(CO)_3\}_8(\mu$-$I)_4$ (**III**).

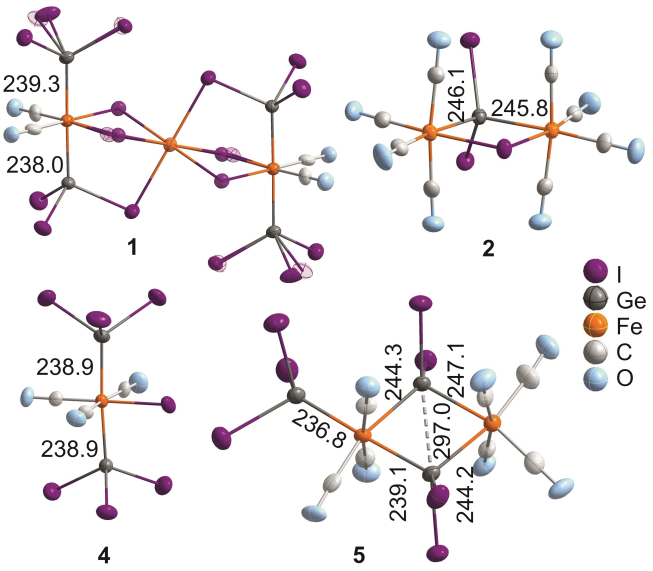

Figure 2. Ge–Fe building units in the novel carbonyl cluster compounds **1**, **2**, **4**, and **5** with selected distances (in pm) (transparent atoms in **1** indicate a reduced site occupancy).

Table 1. Crystallographic data of the Ge–Fe carbonyl cluster compounds **1**–**6**.

	1	2	3	4	5	6
Empirical formula	$C_{20}H_{30}N_4O_4I_{15.5}Fe_{2.75}Ge_4$	$C_{16}H_{15}N_2O_8Cl_8I_3Al_2Fe_2Ge$	$C_8O_8Br_{12}I_3Al_3Fe_3Ge_3$	$C_9H_{11}N_2O_3I_7FeGe_2$	$C_{12}H_9N_2O_7I_7Fe_2Ge_3$	$C_8H_9N_2O_3I_7FeGe_2$
Formula weight (g mol^{-1})	2801.4	1265.9	1884.8	1284.5	1511.0	1270.5
Crystal system	monoclinic	triclinic	triclinic	monoclinic	triclinic	monoclinic
Space group	*P2$_1$/c*	*P-1*	*P-1*	*P2$_1$/n*	*P-1*	*P2$_1$/c*
Lattice parameters,						
a (pm)	1116.4(1)	1086.2(2)	1150.5(2)	981.9(1)	1051.9(2)	997.6(1)
b (pm)	2020.7(1)	1234.9(3)	1278.7(2)	1136.2(1)	1123.8(2)	1840.1(1)
c (pm)	1386.4(1)	1522.2(3)	1379.5(2)	2401.8(1)	1473.7(2)	1441.0(1)
α (°)		89.29(3)	78.29(1)		67.84(1)	
β (°)	112.68(1)	73.65(3)	89.26(1)	98.49(2)	88.78(1)	104.35(1)
γ (°)		78.78(3)	89.95(2)		88.58(1)	
Cell volume ($pm^3 \times 10^6$), V	2885.8	1919.7	1987.0	2650.1	1612.8	2562.7
Formula units per cell, Z	2	2	2	4	2	4
Calculated density (g cm^{-3}),	3.224	2.190	3.150	3.220	3.111	3.293
Measurement limits	$-13 \le h \le 13$, $-21 \le k \le 24$, $-17 \le l \le 17$	$-13 \le h \le 13$, $-11 \le k \le 15$, $-18 \le l \le 18$	$-14 \le h \le 14$, $-15 \le k \le 15$, $-16 \le l \le 16$	$-13 \le h \le 13$, $-15 \le k \le 15$, $-32 \le l \le 32$	$-14 \le h \le 12$, $-15 \le k \le 15$, $-19 \le l \le 19$	$-13 \le h \le 13$, $-25 \le k \le 25$, $-17 \le l \le 19$
Theta range for data collection (°)	3.8 to 52.0	4.0 to 52.0	4.0 to 52.0	3.4 to 58.5	3.9 to 52.0	3.7 to 58.6
Measurement temperature T (K)	200(2)	200(2)	213(2)	200(2)	200(2)	200(2)
Linear absorption coefficient μ (mm^{-1})	11.046	4.576	16.314	10.959	10.372	11.331
Number of reflections	13753 (6044 independent)	10822 (6927 independent)	18427 (7161 independent)	25819 (7016 independent)	10671 (5546 independent)	6823 (5139 independent)
Merging, R_{int}	0.0622	0.0476	0.0434	0.0567	0.0670	0.0509
Number of parameters	259	381	343	219	287	210
Residual electron density ($e^- \times 10^{-6}$ pm^{-3})	−0.98 to 1.32	−0.49 to 0.61	−1.76 to 1.99	−1.67 to 1.76	−2.80 to 2.58	−2.80 to 2.58
Figures of merit[a]						
R1 ($I \ge 2\sigma$)	0.0466	0.0343	0.0574	0.0278	0.0633	0.0401
R1 (all data)	0.0885	0.0766	0.1117	0.0451	0.0868	0.0606
wR2 (all data)	0.0917	0.0501	0.1250	0.0710	0.1902	0.0952
GooF	1.037	0.867	0.807	0.933	1.039	1.016

[a] Figures of merit: $R1 = \Sigma \, | \, |F_o| - |F_c| \, | / \Sigma \, |F_o|$, $wR_2 = \Sigma w(|F_o|^2 - |F_c|^2)^2 / \Sigma w |F_o|2)^{1/2}$, $GooF = S = [\Sigma w(|F_o|^2 - |F_c|^2)^2/(n-p)]^{1/2}$

agreement with the expected ratio (4:2.75:15.5) and clearly indicates a lower amount of Fe and I compared to the stoichiometric formula (4:3:16).

The $[(FeI_2)_{0.75}\{Fe(CO)_2I(GeI_3)_2\}_2]^{2-}$ anion consists of two $Fe(CO)_2I(GeI_3)_2$ subunits, which are linked by a $FeI_{6/2}$ unit. To our surprise, this $FeI_{6/2}$ unit is only partially occupied by 75 %, which is confirmed by single-crystal structure analysis as well as by EDXS. The $Fe(CO)_2I(GeI_3)_2$ subunits exhibit a barbell-shaped Ge_2Fe cluster core with Ge–Fe distances of 238.0(2) (Ge2–Fe1) and 239.3(2) pm (Ge1–Fe1) (Table 2, Figure 2). These distances fit well with Ge–Fe single bonds in similar structural motives, such as in $\{GeI_3\}_2Fe(CO)_4$ with 241.2 pm or 242.0 pm in

Table 2. Assumed valence states of Fe and Ge and selected distances (in pm) for **1**–**6** (for **1** without disorder).

Compound	Ge valence states	Fe valence states	Ge–Fe distances	Ge–I distances	Fe–I distances
$\{GeI_3\}_2Fe(CO)_4$ (**I**)[12]	+III	0	241.2	253.9–255.5	/
$FeI_4\{GeI_3Fe(CO)_3\}_2$ (**II**)[12]	+III	+I/+II ($FeI_{6/2}$)	242.0	253.7–261.6	278.2–289.4
$Ge_{12}\{Fe(CO)_3\}_8(\mu\text{-}I)_4$ (**III**)[9]	0, +I, +II	-I	230.1–245.8	267.1–286.0	/
$[BMIm]_2[(FeI_2)_{0.75}\{Fe(CO)_2I(GeI_3)_2\}_2]$ (**1**)	+III	0, +II ($FeI_{6/2}$)	238.0(2), 239.3(2)	257.4(3)–261.381)	264.4(2)-291.9(1)
$[BMIm][GeI_2\{Fe(CO)_4\}_2(\mu\text{-}I)][AlCl_4]_2$ (**2**)	+II	+I	245.8(1), 246.1(1)	254.1(1), 254.6(1)	263.2(1), 263.7(1)
$[GeI_2\{Fe(CO)_4\}_2(\mu\text{-}I)][Fe(AlBr_4)_3]$ (**3**)	+II	+I	245.5(2), 246.4(2)	251.1(2), 252.7(2)	262.2(2), 262.5(2)
$[EMIm][\{GeI_3\}_2Fe(CO)_3I]$ (**4**)	+III	0	238.9(1)	255.5(1)–259.9(1)	261.7(1)
$[EHIm][Fe(CO)_4(GeI_2)_2Fe(CO)_3GeI_3]$ (**5**)	GeI_3: +III, GeI_2: +II	$Fe(CO)_3$: −I, $Fe(CO)_4$: ±0	236.8(2)-247.1(2)	257.1(2)–260.7(2)	/
$[EMIm][\{GeI_3\}_2Fe(CO)_3I]$ (**6**)	+III	0	238.4(1), 239.0(1)	255.6(1)–258.6(1)	262.5(1)

$FeI_4\{GeI_3Fe(CO)_3\}_2$.[12] Each of the Fe atoms in the $Fe(CO)_2I(GeI_3)_2$ subunits is coordinated to two CO ligands, two GeI_3 groups, one iodine atom (I8: 267.6(5), I8 A: 255(1) pm), and an additional iodine atom (264.4(2) pm) of the sub-stoichiometrically occupied central $FeI_{6/2}$ unit, resulting in a distorted octahedral coordination of Fe1. The Ge–I distances range between 257.4(3) and 261.3(1) pm (Table 2) and are very comparable to those in $\{GeI_3\}_2Fe(CO)_4$ (**I**),[12] $FeI_4\{GeI_3Fe(CO)_3\}_2$ (**II**),[12] or GeI_4 (257 pm).[19] Finally, the Ge–Fe–Ge angle in the $Fe(CO)_2I(GeI_3)_2$ subunits (178.9(1)°) deviates only slightly from 180°.

The central Fe2 atom of the $[(FeI_2)_{0.75}\{Fe(CO)_2I(GeI_3)_2\}_2]^{2-}$ anion is coordinated by two iodine atoms of two opposite GeI_3 groups (291.9(1) pm) and four iodine atoms that are connected by the two Fe1 atoms (276.4(1), 286.8(3) pm, Table 2) of the $Fe(CO)_2I(GeI_3)_2$ subunits, resulting in a distorted octahedral coordination also for Fe2. Fe2 and both two adjacent iodine atoms (2×I7) exhibit site-occupation parameters of only 75%. Consequently, the additional two iodine atoms (I8) that interlink Fe1 and Fe2 exhibit two possible positions with 75% (I8) and 25% (I8 A) probability of finding (Figure 2). Moreover, both GeI_3 groups that are not connected to the central Fe atom (Fe2) also show disorder with two different positions for two of the iodine atoms (I2, I3). Together with the lability of the compound, we assume **1** to be highly metastable and to formally decompose under release of FeI_2 to an $FeI(CO)_2(GeI_3)_2$ intermediate, which is soluble in the IL. Thereafter, $Fe(CO)_4\{GeI_3\}_2$ is most probable formed as less soluble and more stable compound.

Structure and connectivity of $[(FeI_2)_{0.75}\{Fe(CO)_2I(GeI_3)_2\}_2]^{2-}$ are similar to the molecular compound $FeI_4\{GeI_3Fe(CO)_3\}_2$ (**II**),[12] which consists of two $GeI_3Fe(CO)_3I$ subunits and which are interlinked by the distorted octahedral $FeI_{6/2}$ group. As a main difference, one CO ligand of each $GeI_3Fe(CO)_3I$ unit in $FeI_4\{GeI_3Fe(CO)_3\}_2$ is substituted in **1** by a GeI_3 group. This results in dianion instead of a non-charged species. Another similarity between **1** and $FeI_4\{GeI_3Fe(CO)_3\}_2$ relates to the fact that $FeI_4\{GeI_3Fe(CO)_3\}_2$ decomposes within one week with formation of red crystals of $Fe(CO)_4\{GeI_3\}_2$.[12] In this regard, **1** is an excellent example of a very metastable compound that can be nevertheless formed and crystallized by ionic-liquid-based synthesis near room temperature, although the activation barrier to the more stable neighboring phases is low.

[BMIm][GeI$_2${Fe(CO)$_4$}$_2$(μ-I)][AlCl$_4$]$_2$ (**2**) was obtained by reaction of GeI_4 and $Fe_2(CO)_9$ in the presence of Ph_3GeCl and in a $[BMIm]Cl:AlCl_3$ mixture with 1:2 to 1:3 ratio. The synthesis results in dark red, almost black crystals (SI: Figure S1). **2** crystallizes in the triclinic space group *P-1* and contains $[GeI_2\{Fe(CO)_4\}_2(\mu\text{-}I)]^+$ cations as well as both $[BMIm]^+$ cations and $[AlCl_4]^-$ anions, stemming from the IL (Table 1, Figure 2). The synthesis can be rationalized by the oxidation of Fe^0 to Fe^{+I} and reduction of Ge^{+IV} to Ge^{+II}:

$$Fe_2(CO)_9 + GeI_4 + [BMIm]^{+2}\,[AlCl_4]^- \rightarrow [BMIm][GeI_2\{Fe(CO)_4\}_2(\mu\text{-}I)][AlCl_4]_2 + CO + I^-$$

Again, the $[BMIm]Cl:AlCl_3$ ratio of $1:\geq 2$ and the presence of Ph_3GeCl are crucial. Upon decreasing the $[BMIm]Cl:AlCl_3$ ratio, compound **1** was formed, whereas the non-charged molecules $FeI_4\{GeI_3Fe(CO)_3\}_2$[12] or $Ge_{12}\{Fe(CO)_3\}_8(\mu\text{-}I)_4$[9] were obtained in absence of Ph_3GeCl. EDXS confirms the composition of **2** with a Fe:Ge:Al:Cl:I ratio of 1.9:1.1:2.2:7.6:3.0 (scaled on I) (expected: 2:1:2:8:3).

The $[GeI_2\{Fe(CO)_4\}_2(\mu\text{-}I)]^+$ cation in **2** consists of a bent $GeFe_2$ string, which is completed to a four-membered ring by an iodine atom (I1) that interlinks the two Fe atoms. The Ge–Fe distances with 245.8(1) (Ge–Fe2) and 246.1(1) pm (Ge–Fe1) are slightly longer than in **1**, but still in agreement with literature data (e.g., $[Ge_{12}\{FeCp(CO)_2\}_8\{FeCp(CO)\}_2]$).[18b] The Fe–Ge–Fe angle is 103.6(1)° and the opposite Fe–I–Fe angle is 94.4(1)°. The central Ge atom is connected to two iodine and two Fe atoms, resulting in a distorted tetrahedral coordination around Ge. The Ge–I distances (254.1(1), 254.6(1) pm) are very comparable to **1**, $\{GeI_3\}_2Fe(CO)_4$ (**I**), or $FeI_4\{GeI_3Fe(CO)_3\}_2$ (**II**) (Table 2).[12] Both Fe atoms are connected to the central Ge atom, four CO ligands, and the interlinking iodine atom (I1), which, in sum, leads to a slightly distorted octahedral coordination. Finally, the Fe–I distances (263.2(1), 263.7(1) pm) again agree with **1** and $FeI_4\{GeI_3Fe(CO)_3\}_2$ (**II**) (Table 2).[12] All distances of the $[BMIm]^+$ cation and the $[AlCl_4]^-$ anion are as expected and therefore not discussed in detail.

[GeI$_2${Fe(CO)$_4$}$_2$(μ-I)][Fe(AlBr$_4$)$_3$] (**3**) was prepared in a 1:3 mixture of [BMIm]Cl and $AlBr_3$ with GeI_4 and $Fe_2(CO)_9$. Although **3** could also be obtained in a 1:1 mixture of [BMIm]Cl and $AlBr_3$, the 1:3 ratio turned out as optimal in regard of the crystal quality and yield of the title compound. Moreover, the equation of formation points to the need of a higher $AlBr_3$ concentration:

$$2\,Fe_2(CO)_9 + 3\,GeI_4 + 3\,[AlBr_4]^- \rightarrow [GeI_2\{Fe(CO)_4\}_2(\mu\text{-}I)][Fe(AlBr_4)_3] + 10\,CO + 2\,GeI_2 + 5\,I^- + Fe^{2+}$$

3 is obtained in the form of orange-red crystals (SI: Figure S1), together with few tiny orange needles of GeI_2. The title compound crystallizes in the triclinic space group *P-1* and – similar to **2** – contains a $[GeI_2\{Fe(CO)_4\}_2(\mu\text{-}I)]^+$ cation. Moreover, **3** contains a novel complex $[Fe(AlBr_4)_3]^-$ anion (Table 2, Figure 3). EDXS validates the composition with an observed Fe:Ge:Al:Br:I ratio of 2.2:2.1:3.2:11.5:3.0 (scaled on I), which matches with the expected ratio (2:2:3:12:3).

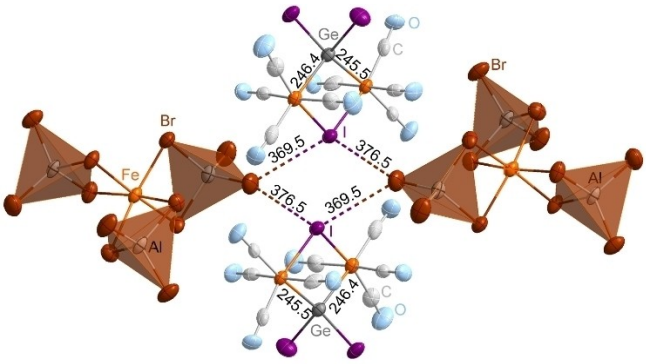

Figure 3. The $[Fe(AlBr_4)_3]^-$ anion with long-ranging Br–Br and Br–I contacts in $[GeI_2\{Fe(CO)_4\}_2(\mu\text{-}I)][Fe(AlBr_4)_3]$ (**3**) with selected bond distances (in pm, $[AlBr_4]^-$ tetrahedra marked by brown color).

Since the $[GeI_2\{Fe(CO)_4\}_2(\mu\text{-}I)]^+$ cation in **3** is similar to compound **2**, it is not discussed again (Table 2). In addition, **3** contains a novel $[Fe(AlBr_4)_3]^-$ anion with a central Fe^{+II} atom (Fe3) that is coordinated by three, distorted tetrahedral $[AlBr_4]^-$ building units (Figure 3). Interestingly, each $[AlBr_4]^-$ shows edge-sharing of two bromine atoms coordinated to the central Fe^{+II}. The Br–Fe–Br angles of adjacent Br atoms range between 83.0(1) (Br6–Fe3–Br5) and 96.5(1)° (Br2–Fe3–Br10). The Br–Fe–Br angles of the *trans*-Br atoms are between 171.8(1) (Br1–Fe3–Br9) and 172.9(1)° (Br5–Fe3–Br10). The Fe–Br distances are observed with 261.1 (Fe3–Br2) to 268.6(1) pm (Fe3–Br5), which is in accordance with literature data (e.g. 267.3 pm in $[FeBr_6]^{2-}$).[20] Due to this specific coordination, short Br–Br contacts of 352.2(2) to 355.7(2) occur between pairs of $[AlBr_4]^-$. This also results in Br–Al–Br angles below the tetrahedral angle (98.0(2)–99.4(1)°) for those Br atoms involved in short Br–Br contacts, whereas other Br–Al–Br angles are increased to 109.5(2)–113.0(2)°. Furthermore, two long-ranging Br–I contacts occur between $[AlBr_4]^-$ tetrahedra and the $[GeI_2\{Fe(CO)_4\}_2(\mu\text{-}I)]^+$ cation (Br4–I1: 369.5(2), 376.5(2) pm (Figure 3) to form a dimeric superordinate $[GeI_2\{Fe(CO)_4\}_2(\mu\text{-}I)][Fe(AlBr_4)_3]$ building unit. These Br–I distances are also below the doubled van-der-Waals distance (Br–Br: 364 pm, Br–I: 380 pm).[21]

[EMIm][Fe(CO)$_3$I(GeI$_3$)] (**4**) was prepared by reacting GeI_4 and $Fe_2(CO)_9$ in the presence of Ph_3GeCl with $[EMIm][NTf_2]$ as IL. The synthesis resulted in dark-red crystals (SI: Figure S1) of the title compound, which crystallizes in the monoclinic space group $P2_1/n$ and contains $[Fe(CO)_3I(GeI_3)]^-$ anions and $[EMIm]^+$ cations from the applied IL (Table 1, Figure 2). The synthesis can be ascribed to the following reaction:

$$Fe_2(CO)_9 + 2\ GeI_4 + [EMIm]^+ \rightarrow [EMIm][Fe(CO)_3I(GeI_3)] + 6\ CO + I^- + Fe^{2+}$$

Beside single crystal structure analysis, the composition was validated by EDXS with a Fe:Ge:I ratio of 0.9:2.2:7 (scaled on I), which coincides with the expectation (1:2:7).

The structure of the $[Fe(CO)_3I(GeI_3)]^-$ anion correlates to the structures of $Fe(CO)_4\{GeI_3\}_2$ (**I**)[12] and the $Fe(CO)_2I(GeI_3)_2$ subunits in **1**. Thus, all contain GeI_3–Fe–GeI_3-type fragments with four CO ligands,[12] three CO and one iodine ligand (**4**), or with two CO and two iodine ligands (**1**) connected to a central Fe atom. The barbell-shaped Ge_2Fe cluster core in **4** exhibits Ge–Fe distances of 238.9(1) pm (Table 2, Figure 2), which are in agreement with Ge–Fe single bonds (e.g., 241.2 pm in $\{GeI_3\}_2Fe(CO)_4$ (**I**) or 242.0 pm in $FeI_4\{GeI_3Fe(CO)_3\}_2$ (**II**)).[12] Again, the Ge–Fe–Ge angle (176.3(1)°) deviates only slightly from a linear arrangement. The Ge–I distances are between 255.5(1) and 259.9(1) pm (Table 2) and very comparable to **1**, **2**, $\{GeI_3\}_2Fe(CO)_4$ (**I**),[12] or $FeI_4\{GeI_3Fe(CO)_3\}_2$ (**II**).[12] The Fe–I distance (261.7(1) pm) fits as well with the compounds **1**, **2**, **3**, and $FeI_4\{GeI_3Fe(CO)_3\}_2$ (**II**).[12]

[EHIm][Fe(CO)$_4$(GeI$_2$)$_2$Fe(CO)$_3$GeI$_3$] (**5**) was synthesized by the reaction of GeI_4 with $Fe_2(CO)_9$ in the presence of Ph_3GeCl and $[NBu_4][BH_4]$ as reducing agent. $[EMIm][NTf_2]$ was used as IL. The synthesis resulted in bright-red crystals of **5** (SI: Figure S1) as minority phase and red crystals of **6** as the main phase. For both phases, moreover, it must be noticed that $[BH_4]^-$ causes a demethylation of the $[EMIm]^+$ cation to $[EHIm]^+$. **5** crystallizes in the triclinic space group *P-1* and consists of $[Fe(CO)_4(GeI_2)_2Fe(CO)_3GeI_3]^-$ anions and $[EHIm]^+$ cations (Table 1, Figure 1). The synthesis can be attributed to the following equation:

$$Fe_2(CO)_9 + 3\ GeI_4 + [EMIm]^+ + 6\ [BH_4]^- \rightarrow [EHIm][Fe(CO)_4(GeI_2)_2Fe(CO)_3GeI_3] + 2\ CO + 5\ I^- + 3\ B_2H_6 + 2.5\ H_2 + CH_4$$

In addition to single-crystal structure analysis, the composition was proven by EDXS (observed Fe:Ge:I ratio: 1.8:3.1:7, scaled on I; expected Fe:Ge:I ratio: 2:3:7).

The $[Fe(CO)_4(GeI_2)_2Fe(CO)_3GeI_3]^-$ anion exhibits a diamond-shaped Ge_2Fe_2 ring with an additional GeI_3 unit connected to one of the Fe atoms, which, in total, results in a Ge_3Fe_2 cluster core. All five metal atoms are almost in plane with a torsion angle below 1.5°. The central Fe atom is connected to two GeI_2 units (239.1(2), 244.2(2) pm) and the additional GeI_3 (236.8(3) pm, Table 2). Moreover, the Fe atom is coordinated to three CO ligands, resulting in a distorted octahedral coordination. Both Ge atoms are bond to two iodine atoms, the already mentioned $Fe(CO)_3$–GeI_3 unit and the $Fe(CO)_4$ unit (244.2(2), 247.1(2) pm). All Ge–I distances are similar to the aforementioned values (Table 2). In the diamond-shaped Ge_2Fe_2 ring, Ge–Fe–Ge angles of 74.4(1) and 75.8(1)° are observed. As a result, the distance between the Ge atoms (297.0(2) pm) is in a range considered as attractive Ge–Ge interaction (e.g. Ge–Ge distances of 296.0 pm in $Ge_{12}\{Fe(CO)_3\}_8(\mu\text{-}I)_4$ (III)).[9] Finally, all Ge atoms exhibit a distorted tetrahedral environment (Figure 2).

[EHIm][Fe(CO)$_3$I(GeI$_3$)] (**6**) was obtained as majority phase in the synthesis of **5**. Again, the $[EMIm]^+$ cation of the IL was demethylated to $[EHIm]^+$ by $[BH_4]^-$. The structure and connectivity of **6** are similar to compound **4** with a $[Fe(CO)_3I(GeI_3)]^-$ anion, but $[EHIm]^+$ instead of $[EMIm]^+$ cations (Table 2). Therefore, **6** is not discussed in detail. In fact, **6** can be assumed to be a more stable decomposition product of **5** and, once more, points to the well-balanced fine-tuning of experimental conditions, which is possible in ILs and which enables a synthesis of a highly metastable intermediate such as **5**.

2.3. Comparison of Synthesis Conditions and Structural Features

Based on nine different carbonyl cluster compounds in the Ge–Fe system, a comparison of the experimental conditions, structural motifs, and stability of the different compounds is possible (Figure 4). Such comparison is rare for highly sensitive and very reactive carbonyls since usually only few compounds are known in a specific system and/or accessible via a specific synthesis route. The here presented Ge–Fe carbonyl cluster compounds, in fact, were all realized by reaction of GeI_4 and $Fe_2(CO)_9$ in ILs at 130 °C. The temperature turned out as less relevant parameter in regard of a controlled formation of the one or other title compound. In fact, the variation of the

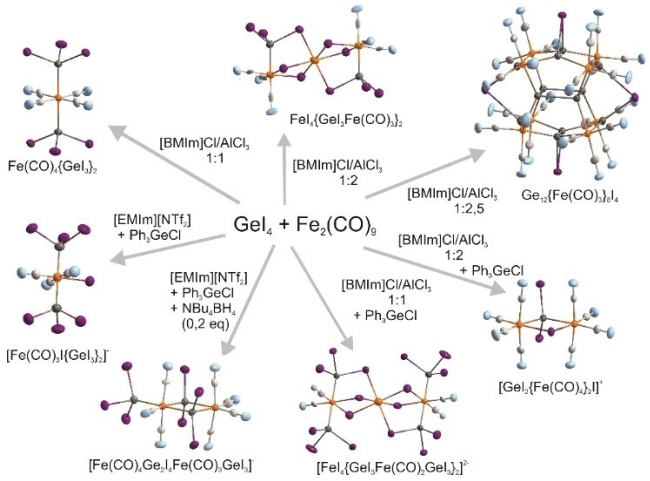

Figure 4. Overview of Ge–Fe carbonyl cluster compounds with their specific conditions of synthesis.

temperature is limited by the incomplete dissolution of the starting materials (e.g., $AlCl_3$, GeI_4) below 130 °C and the beginning $Fe_2(CO)_9$-driven decomposition of the IL above 130 °C.

In addition, the stoichiometric ratio of GeI_4:Ph_3GeCl:Fe_2CO_9 was kept constant at 1:1:2, since higher amounts of GeI_4 just result in a recrystallization of GeI_4 subsequent to the synthesis. Higher amounts of $Fe_2(CO)_9$, moreover, promote the decomposition of the imidazolium cation of the IL. Consequently, the temperature as well as the stoichiometric ratio were identical for all title compounds, which allows a good comparison of the additional experimental conditions. Whereas Ph_3GeCl was absent for the synthesis of the compounds **I–III**, it was used in the synthesis of compounds **1**–**6** to influence the Ge:I ratio.

First of all, a decisive parameter to influence the realization of a specific carbonyl cluster compound in the Ge–Fe system relates to the type, and especially, to the Lewis acidity of the IL (Figure 4). Already for the previously reported compounds, we have observed that $(GeI_3)_2Fe(CO)_4$ (**I**) was obtained with a 1:1 mixture of [BMIm]Cl/$AlCl_3$.[12] Upon increasing the amount of $AlCl_3$ to a 1:2 a mixture of [BMIm]Cl/$AlCl_3$, $GeI_3Fe(CO)_3\}_2FeI_4$ (**II**) was formed.[12] A 1:3 mixture of [BMIm]Cl/$AlCl_3$, finally, resulted in $Ge_{12}\{Fe(CO)_3\}_8(\mu\text{-}I)_4$ (**III**).[9] Since the formation of $[AlCl_4]^-$ is limited to a [BMIm]Cl:$AlCl_3$ ratio <1, moreover, an excess of $AlCl_3$ tends to coordinate I^- stemming from GeI_4. This promotes the formation of Ge–Ge and Ge–Fe bonds as well as the formation of μ^2-bridged iodine atoms between those metals with metal-metal bonds. In contrast, no μ^2-bridged iodine atoms were observed, if acid-base neutral ILs with $[NTf_2]^-$ anions were applied. It should also be noticed that the influence of the Lewis acidity is a characteristic feature of $AlCl_3$. For $AlBr_3$, a similar effect was not observed, which can be attributed a formation of the more stable Al_2Br_6 dimer and the larger size of Br^- in comparison to Cl^-. Hence, a formation of $[AlCl_3I]^-$ as a species dissolved in the IL is obviously preferred in comparison to $[AlBr_3I]^-$.

Based on comparable experimental conditions, the role of Ph_3GeCl can be discussed as additional decisive parameter. Upon dissolution, Ph_3GeCl releases the nucleophilic chloride anion, which already results in a shift of the Lewis-acid-base equilibrium. In addition, the Ph_3Ge^+ cation itself binds iodine to form Ph_3GeI, which reduces the concentration of available iodine in the IL. As a result, the presence of Ph_3GeCl also promotes the formation of Ge–Fe bonds. Since Ph_3GeI is less soluble in the IL than Ph_3GeCl, finally, Ph_3GeI crystallizes all the more as a side phase after the synthesis the more Ph_3GeCl was added.

In regard of the stability of the nine as-prepared Ge–Fe cluster compounds (Figure 5), those containing Ge–Fe–Ge strings turned out to be most stable (i.e., $\{GeI_3\}_2Fe(CO)_4$ (**I**), $[\{GeI_3\}_2Fe(CO)_3I]^-$ (**4**,**6**)). This observation is in accordance with those structural building units that were first identified by *Kummerer* and *Graham* in the 1960s.[14a] All other Ge–Fe carbonyl cluster compounds are much more reactive and typically decompose within days or weeks. Especially $[BMIm]_2[(FeI_2)_{0.75}\{Fe(CO)_2I(GeI_3)_2\}_2]$ (**1**), $FeI_4\{Ge_3Fe(CO)_3\}_2$ (**II**),[12] and [EHIm][$Fe(CO)_4(GeI_2)_2Fe(CO)_3GeI_3$] (**5**) turned out to be highly metastable and decompose even in the mother lye within some days after synthesis. The decomposition usually occurs with the dissolution in the IL and partial release of CO and results in a re-crystallization of the more stable Ge–Fe species $[\{GeI_3\}_2Fe(CO)_3I]^-$ (**4**,**6**) or $\{GeI_3\}_2Fe(CO)_4$ (**I**).

As a general trend, those Ge–Fe carbonyl cluster compounds containing metal atoms that are only connected via iodine (i.e., **II**,**1**) are the least stable. Compounds with μ^2-bridging iodine between the metal atoms turned out to be more stable (i.e., **III**,**2**,**3**). Most stable are those compounds without any bridging iodine atoms (i.e., **I**,**4**,**6**). In addition to the influence of iodine, another general trend relates to the preference of GeI_3–$Fe(CO)_xI_{4-x}$–GeI_3 strings (x = 2–4) for steric reasons. Ring-type building units (i.e. in **5**) or lager cluster cores (i.e. in **III**) are obviously less preferred, which can be attributed to ring strain and less favorable bond angles (e.g., Ge–Fe–Ge angles of 74.4(1) and 75.8(1)° in **5**). The accessibility of all the different carbonyl cluster compounds at comparable exper-

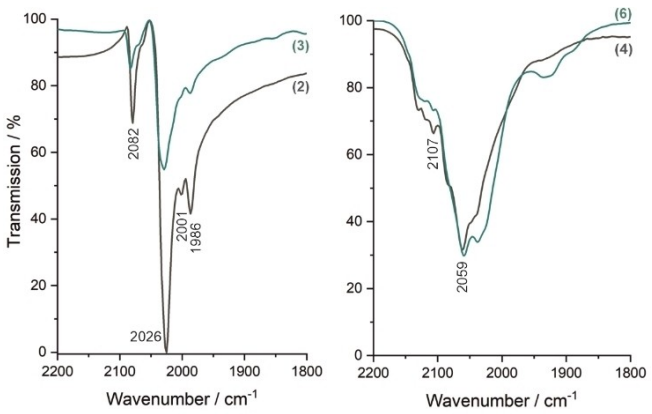

Figure 5. Comparison of the CO vibrations of the Ge–Fe carbonyl cluster compounds **2**,**3**,**4**,**6** according to FT-IR spectroscopy with selected vibrations of **2** and **4**.

imental conditions of course also points out the essential role of ILs that allow a tailored synthesis near room temperature under kinetic reaction control with low activation barriers between the different phases.

The formation of the different Ge–Fe cluster compounds is essentially driven by the redox reaction of GeI_4 and $Fe_2(CO)_9$. Thus, Ge^{+IV} is mostly reduced to Ge^{+II} (except for $Ge_{12}\{Fe(CO)_3\}_8(\mu\text{-}I)_4$ (**III**) containing Ge^0, Ge^{+I}, Ge^{+II}), whereas Fe^0 is oxidized either to Fe^{+I} or to Fe^{+II} (Table 2). Consequently, the use of GeI_2 as the starting material only yields in the recrystallization of orange needles of GeI_2. If it is intended to maintain iron in a zero-valent oxidation state, the addition of $[BH_4]^-$ as a reducing agent turned out to be a suitable measure. This results in the formation of $[EHIm][Fe(CO)_4(GeI_2)_2Fe(CO)_3GeI_3]$ (**5**) with iron in the formal oxidation states 0 and –I (Table 2). However, larger amounts of $[BH_4]^-$ cause a demethylation of the IL-cation, if not a complete decomposition of the imidazolium cation at higher concentration and/or temperature.

In addition to structures and stability of the title compounds, the carbonyl vibrations of **2**,**3**,**4** and **6** were characterized by Fourier-transform infrared spectroscopy (FT-IR) (Table 3, Figure 5, SI: Figure S2). Compound **1** and **5** turned out to be highly labile intermediates and could not be isolated and characterized via FT-IR spectroscopy. As expected, the CO vibrations of **2** and **3** as well as of **4** and **6** are very similar. **2** exhibits a broad absorption at 2059 cm^{-1} with shoulders at 2120, 2107, 2037 and 1935 cm^{-1}. Compared to $Fe_2(CO)_9$ (2084, 2034 cm^{-1}),[22] these vibrations are shifted to higher wavelength. This indicates a weaker back donation and a positive oxidation state of iron, which is in agreement with the assumption from the crystal structure analysis. Similarly, **3** exhibits a broad absorption at 2061 cm^{-1} with shoulders at 2130, 2119, 2106 and 2039 cm^{-1}. The most intense vibrations of **4** are at 2082 and 2026 cm^{-1} with shoulders at 2001 and 1986 cm^{-1} (Table 3, Figure 5). Compared to $Fe_2(CO)_9$ (2084, 2034 cm^{-1}),[22] these vibrations fit well with zero-valent iron, which was assumed as formal valence state based on charge neutrality and bonding situation. In comparison, **6** shows a similar behavior with intense absorptions at 2077 and 2029 cm^{-1} as well as a shoulder at 1987 cm^{-1} (Table 3, Figure 5).

2.4. Formation of Ge–Fe Nanoparticles

Due to their low thermal stability in combination with the release of CO and soluble metal iodides, Ge–Fe carbonyl cluster compounds can serve as potential precursors to obtain bimetallic Ge–Fe nanoparticles at moderate temperatures (< 200 °C). In fact, a rapid thermal decomposition – in accordance with the LaMer-Dinegar model of particle nucleation and particle growth[23] – is optimal to obtain small-sized nanoparticles with narrow size distribution. Since the thermal decomposition can be performed in the IL, moreover, bimetallic nanoparticles are directly accessible in the liquid phase, which allows obtaining non-agglomerated nanoparticles and colloidally stable suspensions. Such strategy to obtain metal nanoparticles by controlled thermal decomposition of metal carbonyls in ILs was already presented by *Janiak et al.* and resulted in a series of high-quality metal nanoparticles.[24]

Although various methods to prepare bimetallic nanoparticles are known, the synthesis is the more demanding the more different the properties of the respective metals. In this regard, the main-group metal germanium and the transition-metal iron are difficult to combine in a single-source precursor. In fact, Ge–Fe nanoparticles were yet only realized by decomposition of $[\{iPrNC(tBu)NiPr\}RGe]Fe(CO)_4$ (R: Cl, N(SiMe$_3$)$_2$),[25] or by heating of $Fe(CO)_5$ and GeI_4 in a mixture of oleylamine and oleic acid.[26] Bimetallic Ge–Fe nanoparticles were nevertheless reported to be interesting as contrast agents for magnetic resonance imaging (MRI) or as ferromagnetic thin films.[25,27]

Here, we have selected $[EMIm][\{GeI_3\}_2Fe(CO)_3I]$ (**4**) as potential single-source precursor, since the compound can be obtained with high purity and high yield (Figures 6,7). After dissolution of **4** in $[BMIm][NTf_2]$, the solution was heated to 80 °C, followed by a rapid addition of a solution of $[NBu_4][BH_4]$ as reducing agent in $[BMIm][NTf_2]$ (Figure 6). Instantaneously, a black suspension was formed indicating the formation of nanoparticles. Finally, the black suspension was heated to 180 °C for 10 min to guarantee complete decomposition of the carbonyl precursor. The resulting suspension was colloidally stable for several days.

The as-prepared Ge–Fe nanoparticles can also be easily extracted from the high-viscous IL via a phase-transfer process (Figure 6). Thus, a solution of oleylamine in *n*-heptane was added as a top-phase. The resulting two-phase system was stirred vigorously for 5 min and then left for additional 20 min at rest. Thereafter, the Ge–Fe nanoparticles were surface-functionalized by oleylamine and transferred to the upper hexane phase (Figure 6). Transmission electron microscopy (TEM) reveals spherical bimetallic nanoparticles with a mean diameter of 7.0 ± 1.4 nm (Figure 7). EDXS indicates a homogenous distribution of both metals and a Ge:Fe ratio of 3:2. According to X-ray powder diffraction the nanoparticles are

Table 3. CO vibrations of the Ge–Fe carbonyl cluster compounds **2**,**3**,**4**,**6** (with strong vibrations in bold).

Compound	CO vibration [cm^{-1}]
$[BMIm][GeI_2\{Fe(CO)_4\}_2(\mu\text{-}I)][AlCl_4]_2$ (**2**)	2120, 2107, **2059**, 2037, 1935
$[GeI_2\{Fe(CO)_4\}_2(\mu\text{-}I)][Fe(AlBr_4)_3]$ (**3**)	2130, 2119, 2106, **2061**, 2039
$[EMIm][\{GeI_3\}_2Fe(CO)_3I]$ (**4**)	**2082**, **2026**, 2001, 1986
$[EHIm][\{GeI_3\}_2Fe(CO)_3I]$ (**6**)	**2077**, **2029**, 1987

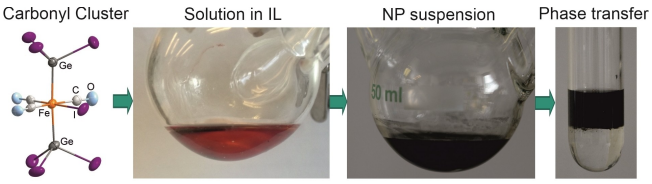

Figure 6. Reaction scheme of the IL-based synthesis of bimetallic Ge–Fe nanoparticles via the decomposition of **4** as single-source precursor.

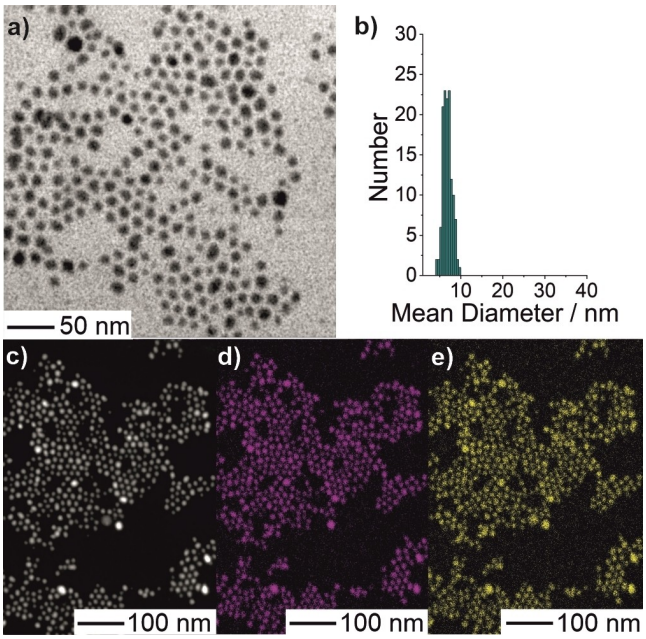

Figure 7. Size, shape and composition of the as-prepared bimetallic Ge–Fe nanoparticles: a) HRTEM image, b) Size distribution, c) HAADF image, d + e) EDXS area scans with Fe (d) and Ge (e) element mappings.

amorphous, which is not a surprise in regard of the small size of the nanoparticles.

3. Conclusions

Altogether nine different germanium-iron carbonyl cluster compounds are prepared via ionic-liquid-based synthesis. This includes $(Fe(CO)_4(GeI_3)_2$, [EMIm][$Fe(CO)_3I(GeI_3)$], and [EHIm][$Fe(CO)_3I(GeI_3)$] with string-type GeI_3–$Fe(CO)_xI_{4-x}$–GeI_3 building units (x = 2–4). $FeI_4\{GeI_3Fe(CO)_3\}_2$ and [BMIm]$_2$[$(FeI_2)_{0.75}\{Fe(CO)_2I(GeI_3)_2\}_2$] also contain such string-like arrangement, which, however, is additionally coupled via iron to pairs. Furthermore, [BMIm][$GeI_2\{Fe(CO)_4\}_2(\mu\text{-}I)$][$AlCl_4$]$_2$, [$GeI_2\{Fe(CO)_4\}_2(\mu\text{-}I)$][$Fe(AlBr_4)_3$], and [EHIm][$Fe(CO)_4(GeI_2)_2Fe(CO)_3GeI_3$] exhibit four-membered Ge_2Fe_2 rings. Finally, $Ge_{12}\{Fe(CO)_3\}_8(\mu\text{-}I)_4$ exhibits the largest cluster core with a $Ge_{12}Fe_8$ building unit.

All these Ge–Fe carbonyl cluster compounds were prepared in ionic liquids using comparable experimental conditions. As a result, the key-parameters to influence and to control the reactions and the formation of the one or other compound could be examined. Here, the Lewis acidity of the applied ionic liquid, the presence/absence of iodine ligands, and the presence/absence of ring-type building units turned out to be most relevant in regard of the formation and stability of the respective compound. [BMIm]$_2$[$(FeI_2)_{0.75}\{Fe(CO)_2I(GeI_3)_2\}_2$] and [EHIm][$Fe(CO)_4(GeI_2)_2Fe(CO)_3GeI_3$] turned out to be most labile intermediates that nevertheless could be crystallized and structurally characterized. In difference, the comparably stable compound [EMIm][$\{GeI_3\}_2Fe(CO)_3I$] could be even used as single-source precursor to obtain bimetallic Ge–Fe nanoparticles with small size and narrow size distribution (7.0 ± 1.4 nm) that were prepared by thermal decomposition of the carbonyl instantaneously in the ionic liquid.

Beside synthesis and characterization of new Ge–Fe carbonyl cluster compounds and the comparison of their structures and stability, the ionic-liquid-based synthesis turned out to be versatile strategy to obtain very labile compounds. In fact, the redox stability, the weakly-coordinating properties, and the inherent stabilization of compounds via cation-anion interactions are essential characteristics of ILs that allow realizing very metastable compounds via a tailored synthesis near room temperature under kinetic reaction control with low activation barriers between the different phases.

Experimental Section

Synthesis

General aspects. All reactions and sample handling were carried out under dried argon atmosphere using standard Schlenk techniques or glove boxes. Reactions were performed in Schlenk flasks and glass ampoules that were evacuated ($p < 10^{-3}$ mbar), heated and flashed with argon three times prior to use. The starting materials GeI_4 (99.99%, ABCR), $Fe_2(CO)_9$ (99%, ABCR), Ph_3GeCl (99%, ABCR), [NBu_4][BH_4] (98%, Sigma Aldrich), $AlCl_3$ (99.9%, Sigma-Aldrich) and $AlBr_3$ (ABCR) were used as received. [BMIm]Cl (99%, Iolitec) was dried under reduced pressure (10^{-3}mbar) at 130 °C for 48 h. The ionic liquid [EMIm][NTf_2] ([NTf_2]$^-$: [$N(SO_2CF_3)_2$]$^-$) was prepared according to literature procedures[28] and dried several days under reduced pressure ($< 10^{-3}$ mbar) at 130 °C before use. Oleylamine (Acros, 80–90%) was stored over activated molecular sieve (3 Å) for at least 30 days and degassed by freeze-pump-thaw cycles. *n*-Heptane (Sigma-Aldrich, 99%) was refluxed and freshly distilled over CaH_2. All compounds were handled and stored in argon-filled glove boxes (MBraun Unilab, $c(O_2, H_2O) < 0.1$ ppm).

The synthesis of $(Fe(CO)_4(GeI_3)_2$ (**I**), $FeI_4\{GeI_3Fe(CO)_3\}_2$ (**II**), and $Ge_{12}\{Fe(CO)_3\}_8(\mu\text{-}I)_4$ (**III**) was reported elsewhere.[9,12]

*[BMIm]$_2$[$(FeI_2)_{0.75}\{Fe(CO)_2I(GeI_3)_2\}_2$] (**1**).* 80 mg (138 mmol) of GeI_4, 50.2 mg (0.138 mmol) of $Fe_2(CO)_9$, 46.8 mg (0.138 mmol) of Ph_3GeCl, 300 mg (1.718 mmol) of [BMIm]Cl and 229 mg (1.718 mmol) of $AlCl_3$ were heated under argon in a sealed glass ampoule for 96 h at 130 °C. After cooling to room temperature with a rate of 1 K/h, **1** was obtained as a side phase in the form of dark-red crystals together with bright red crystals of Ph_3GeI. **1** is very sensitive to air and moisture and needs to be handled under inert conditions. Single crystals were manually separated by crystal picking. Due the fact that **1** is a side-product, its yield was estimated to about 5%.

*[BMIm][$GeI_2\{Fe(CO)_4\}_2(\mu\text{-}I)$][$AlCl_4$]$_2$ (**2**).* 80 mg (0.138 mmol) of GeI_4, 50.2 mg (0.138 mmol) of $Fe_2(CO)_9$, 46.8 mg (0.138 mmol) of Ph_3GeCl, 300 mg (1.718 mmol) of [BMIm]Cl and 458 mg (3.435 mmol) of $AlCl_3$ were heated under argon in a sealed glass ampoule for 96 h at 130 °C. After cooling to room temperature with a rate of 1 K/h, **2** was obtained as dark-red needles with a yield of about 40%. **2** is sensitive to air and moisture and needs to be handled under inert conditions. Single crystals of **2** were separated from the mother lye by filtration through a glass filter.

*[$GeI_2\{Fe(CO)_4\}_2(\mu\text{-}I)$][$Fe(AlBr_4)_3$]$_2$ (**3**).* 160 mg (0.276 mmol) of GeI_4, 100.4 mg (0.276 mmol) of $Fe_2(CO)_9$, 300 mg (1.718 mmol) of [BMIm]-Cl and 1374.1 mg (5.153 mmol) of $AlBr_3$ were heated under argon in a sealed glass ampoule for 96 h at 130 °C. After cooling to room temperature with a rate of 1 K/h, **3** was obtained as orange-red crystals together with few tiny orange needles of GeI_2. **3** is sensitive

to air and moisture and needs to be handled under inert conditions. Single crystals for characterization were manually separated by crystal picking. The yield of **3** was estimated to about 20%.

*[EMIm][Fe(CO)$_3$I(GeI$_3$)$_2$] (**4**).* 80 mg (0.138 mmol) of GeI_4, 50.2 mg (0.138 mmol) of $Fe_2(CO)_9$, 46.8 mg (0.138 mmol) of Ph_3GeCl and 1 mL of [EMIm][NTf_2] were heated under argon in a sealed glass ampoule for 96 h at 130 °C. After cooling to room temperature with a rate of 1 K/h, **4** was obtained as dark-red blocks with a yield of about 70%. **4** is sensitive to air and moisture and needs to be handled under inert conditions. For characterization, crystals of **4** were separated from the mother lye by filtration through a glass filter.

*[EHIm][Fe(CO)$_4$(GeI$_2$)$_2$Fe(CO)$_3$GeI$_3$] (**5**).* 100 mg (0.172 mmol) of GeI_4, 62.7 mg (0.127 mmol) of $Fe_2(CO)_9$, 11.7 mg (0.025 mmol) of Ph_3GeCl, 8.9 mg (0.025 mmol) of [NBu_4][BH_4] and 1 mL of [EMIm][NTf_2] were heated under argon in a sealed glass ampoule for 96 h at 130 °C. After cooling to room temperature with a rate of 1 K/h, **5** was obtained as a minor side phase as bright-red crystals together with crystals of [EHIm][{GeI_3}$_2$Fe(CO)$_3$I] as the main phase. **5** is very sensitive to air and moisture and needs to be handled under inert conditions. Single crystals were manually separated by crystal picking. The yield of **5** was estimated to about 5%.

*[EHIM][Fe(CO)$_3$I(GeI$_3$)] (**6**).* 100 mg (0.172 mmol) of GeI_4, 62.7 mg (0.127 mmol) of $Fe_2(CO)_9$, 11.7 mg (0.025 mmol) of Ph_3GeCl, 8.9 mg (0.025 mmol) of [NBu_4][BH_4] and 1 mL of [EMIm][NTf_2] were heated under argon in a sealed glass ampoule for 96 h at 130 °C. After cooling to room temperature with a rate of 1 K/h, **6** was obtained as main phase as red crystals together with bright crystals of [EHIm][{GeI_3}$_2$Fe(CO)$_3$I] as a side phase. **6** is sensitive to air and moisture and needs to be handled under inert conditions. Single crystals for characterization were manually separated by crystal picking. The yield was estimated to about 30%.

Bimetallic Ge–Fe nanoparticles. 50 mg (0.039 mmol, 1 eq) of [EMIm][Fe(CO)$_3$I(GeI$_3$)$_2$] (**4**) were dissolved in 5 mL of [BMIm][NTf_2] at 80 °C. After dissolution, 30.0 mg of [NBu_4][BH_4] (0.117 mmol, 3 eq) dissolved in 2.5 mL of [BMIm][NTf_2] were added quickly. Afterwards, the instantaneously formed black suspension was heated to 180 °C for 10 min. After cooling to room temperature, the nanoparticles were either centrifuged and washed three-times with acetonitrile, followed by drying under reduced pressure to obtain powder samples. Alternatively, the bimetallic nanoparticles were extracted by phase transfer to obtain stable suspensions. Therefore, 5 mL of *n*-heptane and 0.5 mL of oleylamine were added to the IL-suspension and stirred vigorously for 5 min. After 20 min, the liquid phases were separated. The bimetallic nanoparticles are now dispersed in the upper *n*-heptane phase.

Analytical equipment

Single-crystal X-ray structure analysis. Suitable crystals were selected by crystal picking and covered by inert-oil (perfluoropolyalkylether, ABCR). Data collection was performed at 200 K on an Stoe IPDS II diffractometer (Stoe, Darmstadt Mo–K_α radiation ($\lambda = 0.71073$ Å, graphite monochromator). Data reduction and multi-scan absorption correction were conducted with the X-AREA software package (version 1.75, Stoe) and STOE LANA (version 1.63.1, Stoe).[29] Space group determination based on systematic absences of reflections, structure solution based on direct methods as well as structure refinement were performed within the software package OLEX2[30] by XPREP and SHELXTL (version 6.14, SHELX-2018).[31] All non-hydrogen atoms were refined anisotropically. Refinement was checked with PLATON.[32] Detailed information on crystal data and structure refinement can be found in the following section. DIAMOND was used for all illustrations.[33] https://www.ccdc.cam.ac.uk/services/structures?id=doi:10.1002/open.202000254 Deposition Numbers 2025775 (for **2**), 2025776 (for **3**), 2025777 (for **4**), 2025778 (for **6**), 2025779 (for **5**) and 2025780 (for **1**) contain the supplementary crystallographic data for this paper. These data are provided free of charge by the joint Cambridge Crystallographic Data Centre and Fachinformationszentrum Karlsruhe Access Structures service https://www.ccdc.cam.ac.uk/structures/.

Fourier-transform infrared (FT-IR) spectra were recorded on a Bruker Vertex 70 FT-IR spectrometer (Bruker). The samples were measured as pellets in KBr. Thus, 300 mg of dried KBr and 0.5–1.0 mg of the sample were carefully pestled together and pressed to a thin pellet.

Energy dispersive X-ray spectroscopy (EDXS) of single crystals was performed using an Ametec EDAX mounted on a Zeiss SEM Supra 35 VP scanning electron microscope. The samples were prepared in the glove-box by selecting single crystals that were fixed on a conductive carbon pad on an aluminum sample holder. The samples were handled under inert conditions during transport and sample preparation. High-resolution EDXS was performed to analyze the chemical composition of nanoparticles. The spectra were obtained at 200 kV electron energy with a FEI Osiris microscope that was equipped with a Bruker Quantax system (XFlash detector). EDX spectra were quantified with the FEI software package "TEM imaging and analysis" (TIA). Using TIA, element concentrations were calculated on the basis of a refined Kramers' law model that includes corrections for detector absorption and background subtraction. Standard quantification, i.e.by means of theoretical sensitivity factors, without thickness correction was applied. EDX spectra were taken in the STEM mode with a probe diameter of 0.5 nm. Using a focused electron probe, EDXS area scans were performed to obtain average compositions of larger sample regions. The EDXS spectra were acquired by continuously scanning the electron probe in the predefined region.

Transmission electron microscopy (TEM) Transmission electron microscopy (TEM) was conducted with a FEI Osiris microscope at 200 kV. TEM samples were prepared by evaporating *n*-heptane suspensions on amorphous carbon (lacey-)film suspended on copper grids. The deposition of the samples on the carbon (lacey-)film copper grids was performed under argon atmosphere in a glovebox. The grids were thereafter transferred with a suitable vacuum/inert gas transfer module into the transmission electron microscope without any contact to air. Average particle diameters were calculated by statistical evaluation of at least 100 particles (ImageJ 1.47v software).

Acknowledgements

The authors thank the Deutsche Forschungsgemeinschaft (DFG) for funding in the Priority Program SPP1708 "Material synthesis near room temperature".

Conflict of Interest

The authors declare no conflict of interest.

Keywords: Ge–Fe systems · cluster compounds · crystal structures · ionic liquids · nanoparticles

[1] P. Wasserscheid, T. Welton, *Ionic Liquids in Synthesis*, Wiley-VCH, Weinheim **2008**.
[2] D. Freudenmann, S. Wolf, M. Wolff, C. Feldmann, *Angew. Chem. Int. Ed.* **2011**, *50*, 11050–11060 (Review).
[3] a) E. Ahmed, M. Ruck, *Dalton Trans.* **2011**, *40*, 9347–9357 (Review); b) M. F. Groh, A. Wolff, M. A. Grasser, M. Ruck, *Int. J. Mol. Sci.* **2016**, *17*, 1452.
[4] A. M. Guloy, R. Ramlau, Z. Tang, W. Schnelle, M. Baitinger, Y. Grin, *Nature* **2006**, *443*, 320–323.
[5] C. Donsbach, K. Reiter, D. Sundholm, F. Weigend, S. Dehnen, *Angew. Chem. Int. Ed.* **2018**, *57*, 8770–8774; *Angew. Chem.* **2018**, *130*, 8906–8910.
[6] M. Knies, M. Kaiser, A. Isaeva, U. Müller, T. Doert, M. Ruck, *Chem. Eur. J.* **2018**, *24*, 127–132.
[7] I. M. Riddlestone, A. Kraft, J. Schaefer, I. Krossing, *Angew. Chem. Int. Ed.* **2018**, *57*, 13982–14024.
[8] S. Wolf, F. Winter, R. Pöttgen, N. Middendorf, W. Klopper, C. Feldmann, *Chem. Eur. J.* **2012**, *18*, 13600–13604.
[9] S. Wolf, W. Klopper, C. Feldmann, *Chem. Commun.* **2018**, *54*, 1217–1220.
[10] S. Wolf, R. Köppe, T. Block, R. Pöttgen, P. W. Roesky, C. Feldmann, *Angew. Chem. Int. Ed.* **2020**, *59*, 5510–5514.
[11] a) S. Wolf, K. Reiter, F. Weigend, W. Klopper, C. Feldmann, *Inorg. Chem.* **2015**, *54*, 3989–3994; b) S. Wolf, D. Fenske, W. Klopper, C. Feldmann, *Dalton Trans.* **2019**, *48*, 4696–4701.
[12] S. Wolf, C. Feldmann, *Z. Anorg. Allg. Chem.* **2017**, *643*, 25–30.
[13] P. Braunstein, L. A. Oro, P. R. Raithby, *Metal Clusters in Chemistry*, Wiley-VCH, Weinheim **2008**.
[14] a) R. Kummerer, W. A. G. Graham, *Inorg. Chem.* **1968**, *7*, 1208–1214; b) J. Barrau, N. B. Hamida, A. Agrebi, J. Satge, *Organometallics* **1989**, *8*, 1585–1593; c) J. Barrau, N. B. Hamida, J. Satge, *J. Organomet. Chem.* **1990**, *387*, 65–76.
[15] a) J. D. Cotton, R. M. Peachey, *J. Inorg. Nucl. Chem.* **1970**, *6*, 727–731; b) W. M. Butler, W. A. McAllister, W. M. Risen, *Inorg. Chem.* **1974**, *13*, 1702–1708.
[16] V. Y. Lee, Y. Ito, H. Yasuda, K. Takanashi, A. Sekiguchi, *J. Am. Chem. Soc.* **2011**, *133*, 5103–5108.
[17] a) S. G. Anema, K. M. Mackay, B. K. Nicholson, *J. Chem. Soc., Dalton Trans.* **1996**, 3853–3858; b) S. G. Anema, K. M. Mackay, B. K. Nicholson, M. van Tiel, *J. Organomet. Chem.* **1990**, *9*, 2436–2442.
[18] a) A. Schnepf, C. Schenk, *Angew. Chem. Int. Ed.* **2006**, *45*, 5373–5346; *Angew. Chem.* **2006**, *118*, 5499–5502; b) C. Schenk, F. Henke, A. Schnepf, *Angew. Chem. Int. Ed.* **2013**, *52*, 1834–1838; *Angew. Chem.* **2013**, *125*, 1883–1887.
[19] a) F. M. Jaeger, P. Terpstra, H. G. K. Westenbrink, *Proc. R. Neth. Acad. Arts Sci.* **1925**, *28*, 747–766; b) L. Walz, D. Thiery, E. M. Peters, H. Wendel, E. Schoenherr, M. Wojnowski, *Z. Kristallogr.* **1993**, *208*, 207–211.
[20] A. V. Olenev, O. S. Oleneva, M. Lindsjö, L. A. Kloo, A. V. Shevelkov, *Chem. Eur. J.* **2003**, *14*, 3201–3208.
[21] M. Mantina, A. C. Chamberlin, R. Valero, C. J. Cramer, D. G. Truhlar, *J. Phys. Chem. A*, **2009**, *113*, 5806–5812.
[22] a) F. A. Cotton, J. M. Troup, *J. Chem. Soc. Dalton Trans.* **1974**, 800–802; b) R. K. Sheline, K. S. Pitzer, *J. Am. Chem. Soc.* **1950**, *72*, 1107–1112.
[23] V. K. LaMer, R. H. J. Dinegar, *J. Am. Chem. Soc.* **1950**, *72*, 4847–4854.
[24] a) S. Wegner, C. Janiak, *Top. Curr. Chem.* **2017**, *375*, 1–32 (Review); b) C. Vollmer, C. Janiak, *Coord. Chem. Rev.* **2011**, *255*, 2039–2057 (Review).
[25] A. Sodreau, S. Mallet-Ladeira, S. Lachaize, K. Miqueu, J.-M. Sotiropoulos, D. Madec, C. Nayral, F. Delpech, *Dalton Trans.* **2018**, *47*, 15114–15120.
[26] D. D. Vaughn, D. Sun, J. A. Moyer, A. J. Biacchi, R. Misra, P. Schiffer, R. E. Schaak, *Chem. Mater.* **2013**, *25*, 4396–4401.
[27] a) P. Zhou, L. Pan, G. Deng, Z. Zhou, H. Zhao, C. Peng, S. Yang, *J. Mater. Chem. B* **2019**, *7*, 5661–5668; b) R. Goswami, G. Kioseoglou, A. T. Hanbicki, O. M. J. Van 't Erve, B. T. Jonker, G. Spanos, *Appl. Phys. Lett.* **2005**, *86*, 032509/1–032509/3; c) Y. K. Wakabayashi, Y. Ban, S. Ohya, M. Tanaka, *Phys. Rev. B* **2014**, *90*, 205209/1–205209/7.
[28] D. R. MacFarlane, P. Meakin, J. Sun, N. Amini, N. Forsyth, *J. Phys. Chem. B* **1999**, *103*, 4164–4170.
[29] J. Koziskova, F. Hahn, J. Richter, J. Kozisek, *Acta Chim. Slov.* **2016**, *9*, 136–140.
[30] O. V. Dolomanov, L. J. Bourhis, R. J. Gildea, J. A. K. Howard, H. Puschmann, *J. Appl. Crystallogr.* **2009**, *42*, 339–341.
[31] a) G. M. Sheldrick, *Acta Crystallogr. Sect. A*, **2008**, *64*, 112–122; b) G. M. Sheldrick, *Acta Crystallogr. Sect. C* **2015**, *71*, 3–8.
[32] a) A. L. Spek, *Acta Crystallogr.* **2009**, *D65*, 148–155; b) A. L. Spek, *Acta Crystallogr.* **2015**, *C71*, 9–18; c) A. L. Spek, *Acta Crystallogr.* **2020**, *E76*, 1–11.
[33] Version 4.2.2: *Crystal and Molecular Structure Visualization*. Crystal Impact GbR, Bonn **2016**.

Manuscript received: September 3, 2020
Revised manuscript received: September 30, 2020